

Cell Reports Physical Science, Volume 6

Supplemental information

**Three-dimensional imaging of the microstructure
of lithium metal anode using Xenon
plasma focused ion beam**

Yueying Peng and Kei Nishikawa

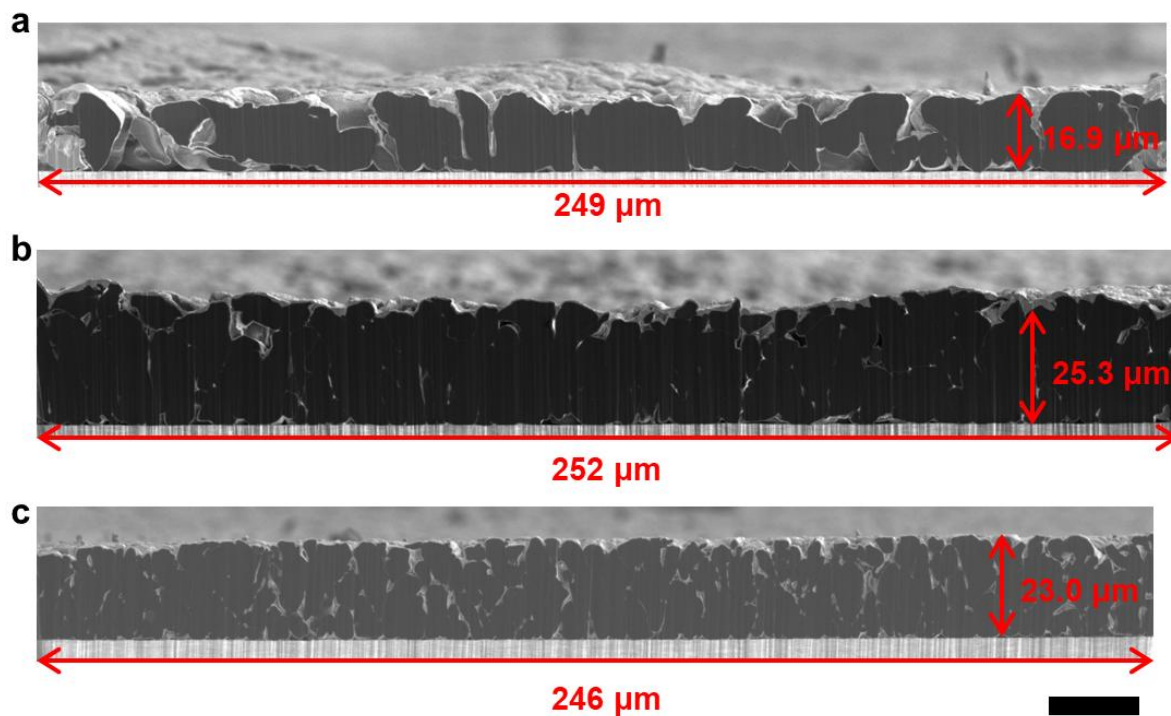


Figure S1. Cross-sectional scanning electron microscopy (SEM) images of the electrodeposited Li after Xenon plasma focused ion beam (Xe PFIB) cross-sectional milling

(a) The electrodeposited Li obtained at 0.2 mA cm^{-2} .

(b) The electrodeposited Li obtained at 0.5 mA cm^{-2} .

(c) The electrodeposited Li obtained at 2 mA cm^{-2} .

The scale bar represents 20 μm , and the capacity of electrodeposited Li is 5 mAh cm^{-2} .

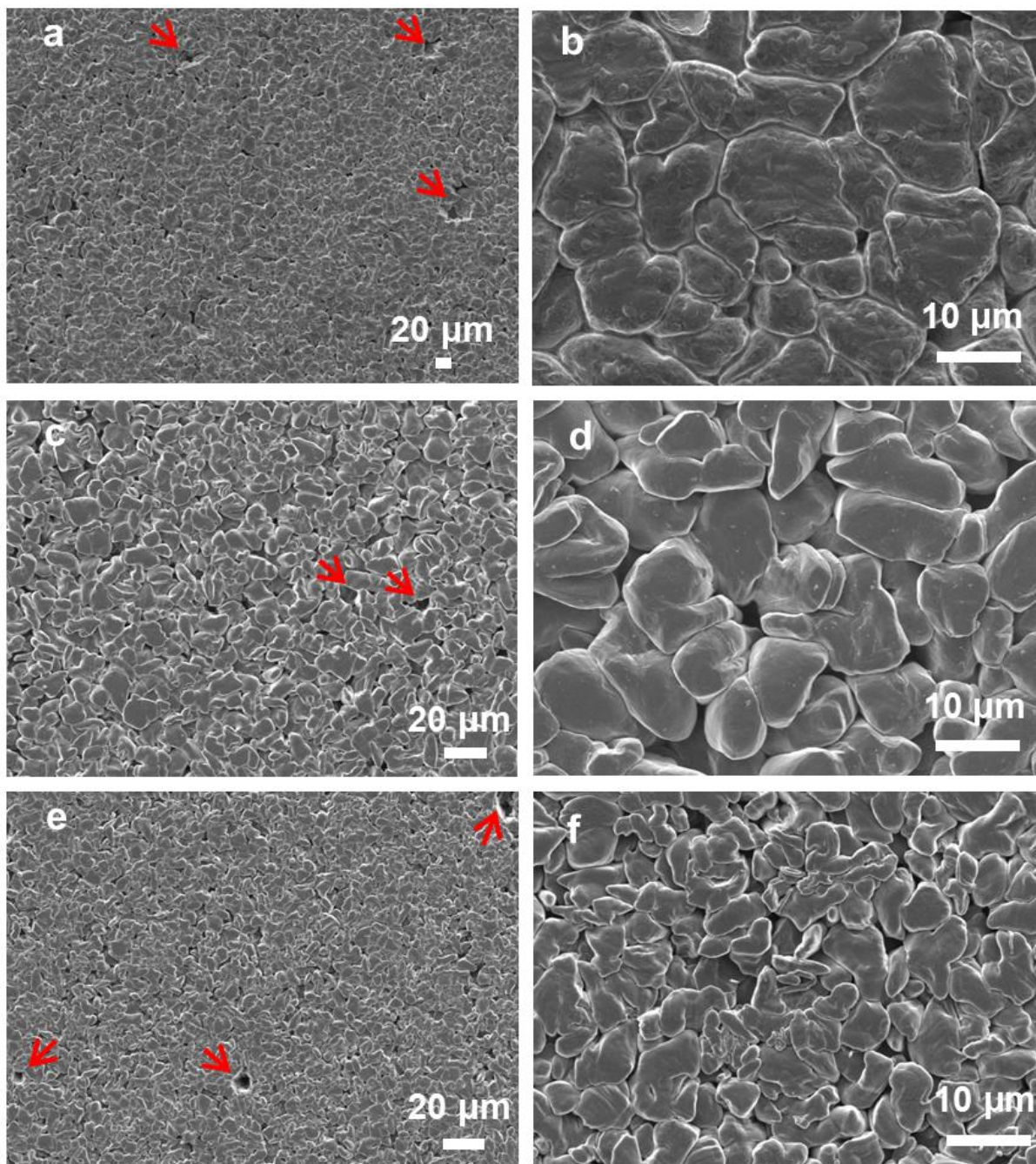


Figure S2. Top-view SEM images of electrodeposited Li metal

(a and b) The electrodeposited Li obtained at 0.2 mA cm^{-2} .

(c and d) The electrodeposited Li obtained at 0.5 mA cm^{-2} .

(e and f) The electrodeposited Li obtained at 2 mA cm^{-2} .

(b, d, f) are the magnified images of (a, c, e), respectively. At the large micron scale in the low-magnification images (a, c, e), microvoids are observed, as indicated by the red arrows.

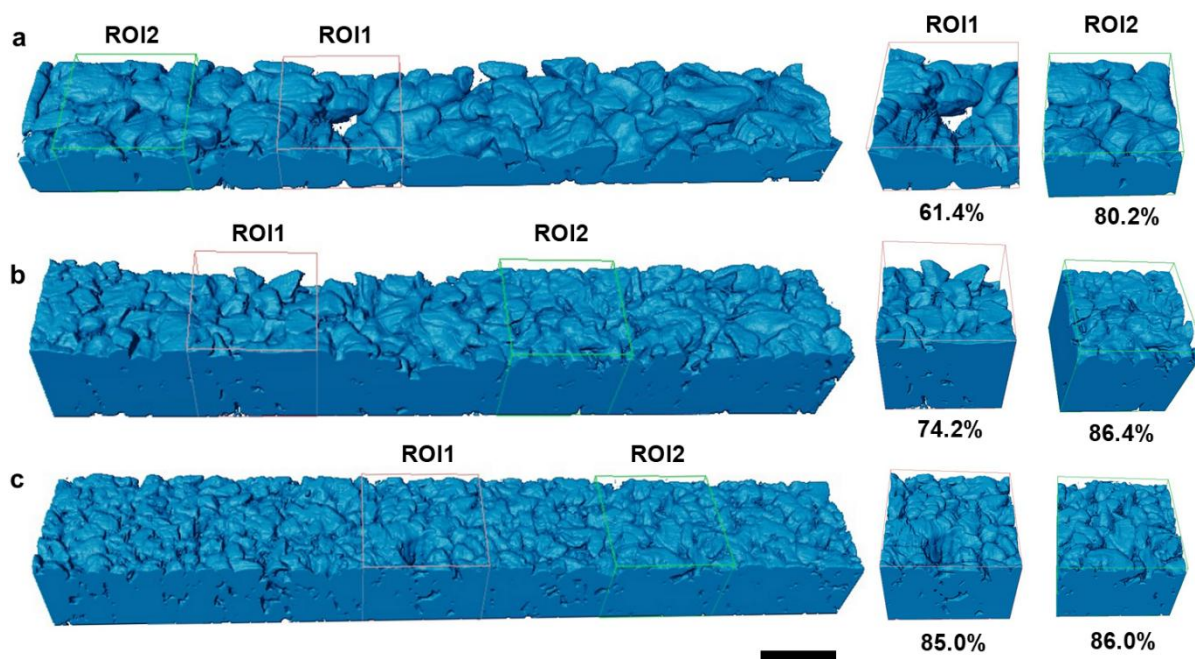


Figure S3. Reconstructed 3D images of metallic Li phases

(a) The electrodeposited Li obtained at 0.2 mA cm⁻².

(b) The electrodeposited Li obtained at 0.5 mA cm⁻².

(c) The electrodeposited Li obtained at 2 mA cm⁻².

The displayed values are the corresponding quantified Li volume fractions of different regions of interest (ROIs) with and without clear microvoids (ROI1 and ROI2, respectively). The scale bar represents 20 μm, and the volumes of the ROIs are controlled at the same dimensions of $x = 25 \mu\text{m}$ and $y = 25 \mu\text{m}$.

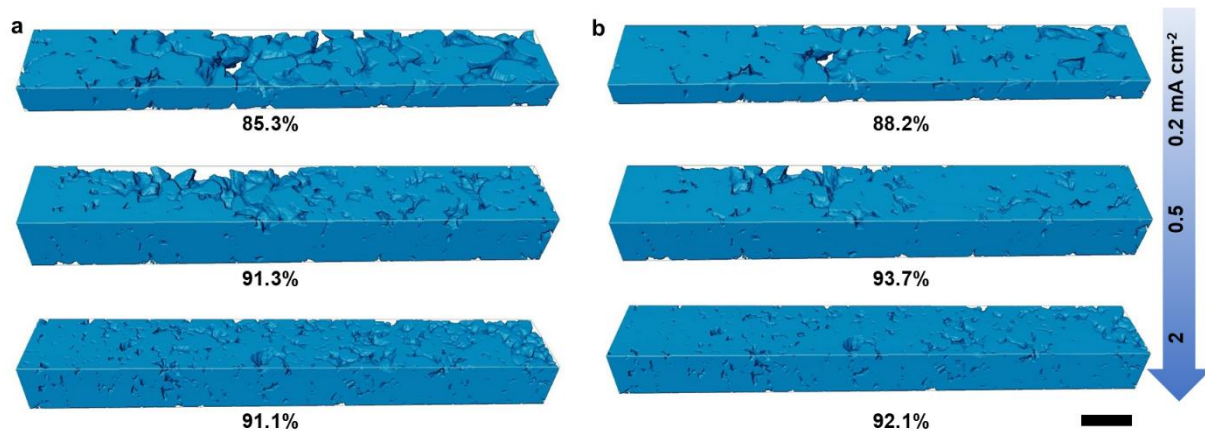


Figure S4. Reconstructed 3D images of metallic Li phases after cutting the surfaces

(a) Cutting the surfaces to Li area fractions of <60%.

(b) Cutting the surfaces to Li area fractions of <80%.

The displayed values are the quantified Li volume fractions. The scale bar represents 20 μm , and the volumes are controlled at the same dimensions of $x = 200 \mu\text{m}$ and $y = 30 \mu\text{m}$.

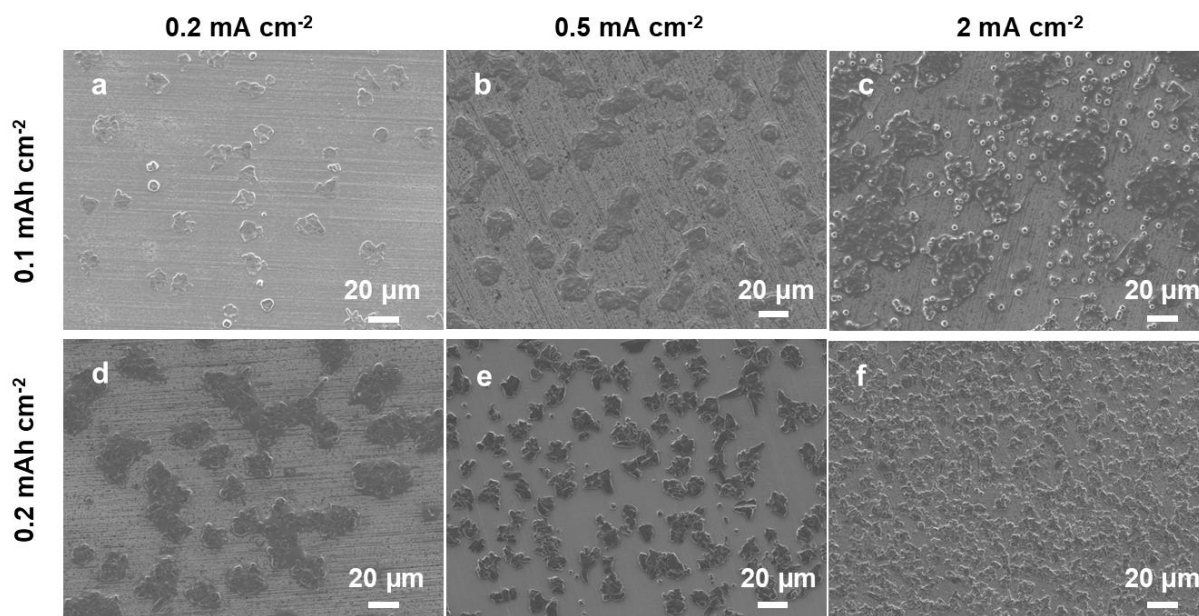


Figure S5. Top-view SEM images of the electrodeposited Li metal

(a–c) 0.1 mAh cm^{-2} of Li electrodeposited at (a) 0.2, (b) 0.5, and (c) 2 mA cm^{-2} .

(d–f) 0.2 mAh cm^{-2} of Li electrodeposited at (d) 0.2, (e) 0.5, and (f) 2 mA cm^{-2} .

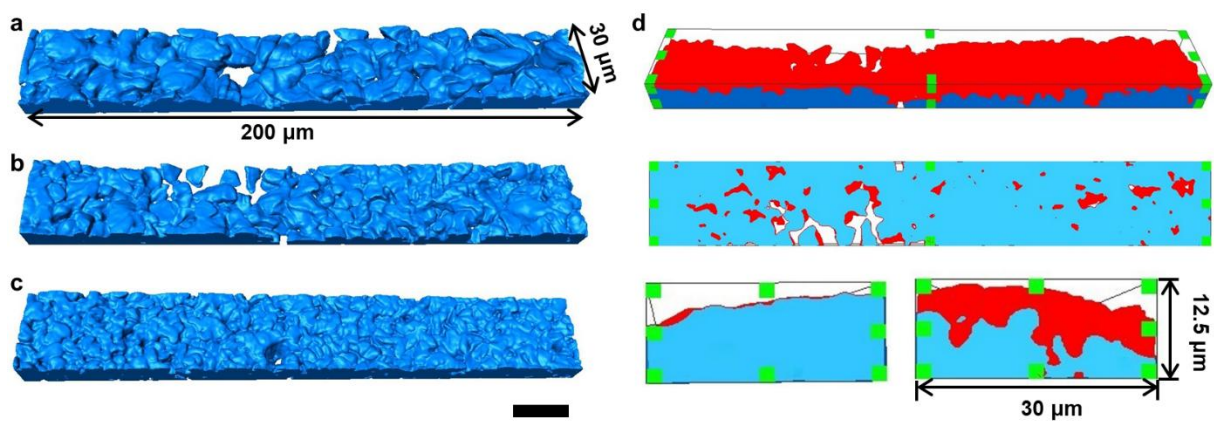


Figure S6. Generated 3D surfaces of electrodeposited Li metal

(a) The electrodeposited Li obtained at 0.2 mA cm^{-2} .

(b) The electrodeposited Li obtained at 0.5 mA cm^{-2} .

(c) The electrodeposited Li obtained at 2 mA cm^{-2} .

(d) Schematic of the calculation of the true surface of the Li/electrolyte interface. Red patch represents the surface of the Li/electrolyte interface.

The scale bar represents $20 \text{ }\mu\text{m}$, and the volumes are controlled at the same dimensions of $x = 200 \text{ }\mu\text{m}$, $y = 30 \text{ }\mu\text{m}$, and $z = 12.5 \text{ }\mu\text{m}$.

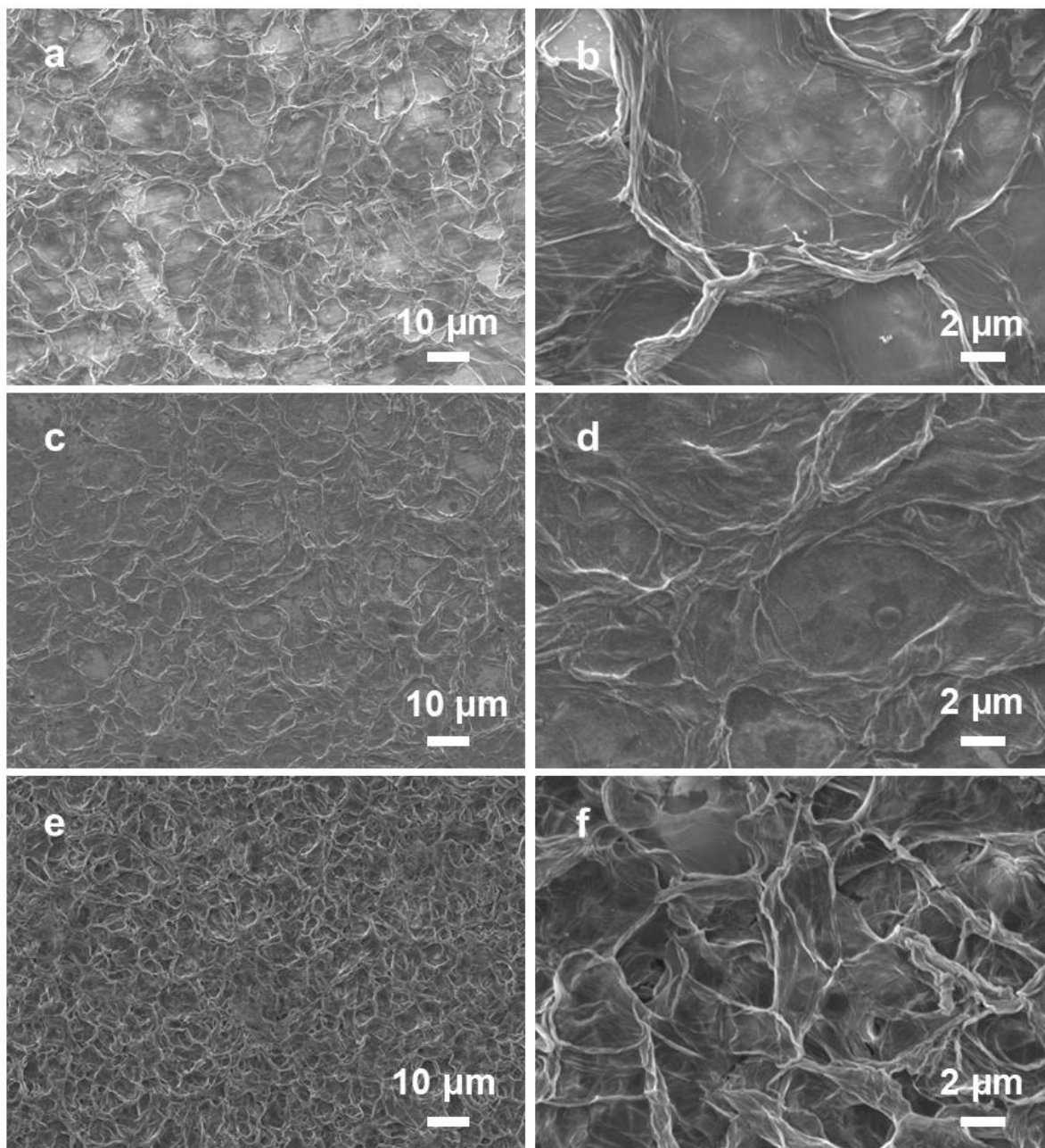


Figure S7. Top-view SEM images of electrodeposited Li after stripping

(a and b) Plating and stripping at 0.2 mA cm^{-2} .

(c and d) Plating and stripping at 0.5 mA cm^{-2} .

(e and f) Plating and stripping at 2 mA cm^{-2} .

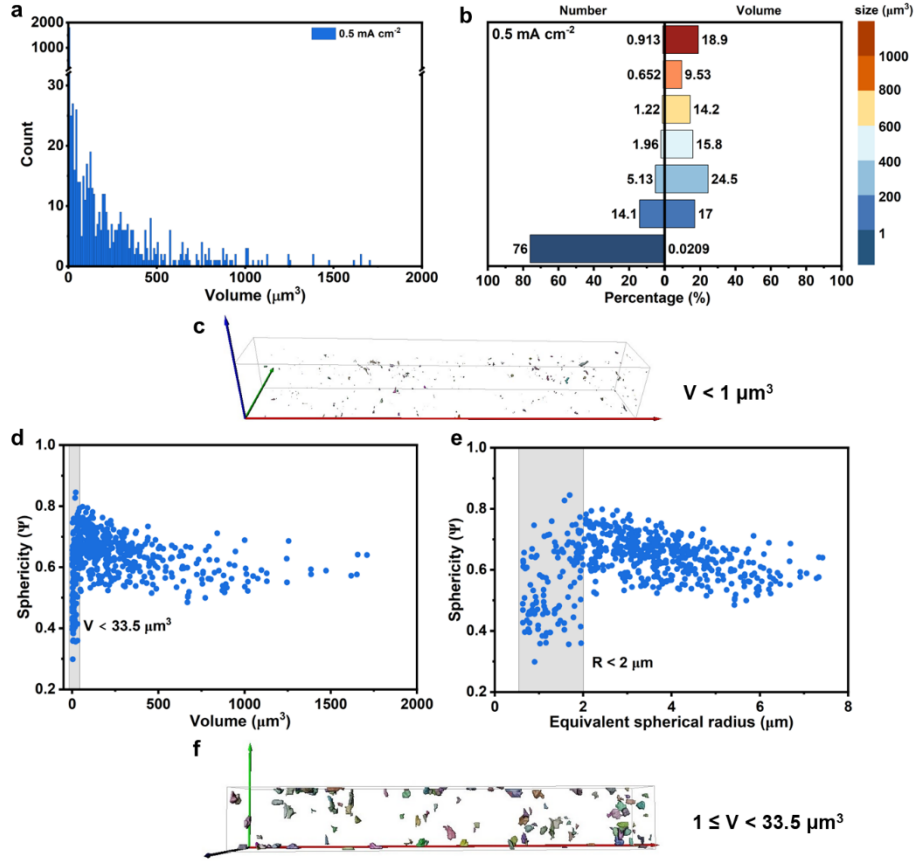


Figure S8. Three-dimensional quantitative analyses of separated Li particles

(a) Histograms of all Li particles.

(b) Volume and number percentages of the Li particles with different volumes (V), which range from $V \geq 1000 \mu\text{m}^3$, $800 \mu\text{m}^3 \leq V < 1000 \mu\text{m}^3$, $600 \mu\text{m}^3 \leq V < 800 \mu\text{m}^3$, $400 \mu\text{m}^3 \leq V < 600 \mu\text{m}^3$, $200 \mu\text{m}^3 \leq V < 400 \mu\text{m}^3$, and $1 \mu\text{m}^3 \leq V < 200 \mu\text{m}^3$ to $V < 1 \mu\text{m}^3$.

(c) Reconstructed 3D images of the Li particles with $V < 1 \mu\text{m}^3$.

(d and e) Dependencies of the sphericity of a Li particle on the (d) volumes and (e) equivalent spherical radius, with $V \geq 1 \mu\text{m}^3$.

(f) Reconstructed 3D images of the Li particles with $1 \mu\text{m}^3 \leq V < 33.5 \mu\text{m}^3$ from the surface view.

The red, green, and blue arrows represent the directions of the x-, y-, and z-axes, respectively.

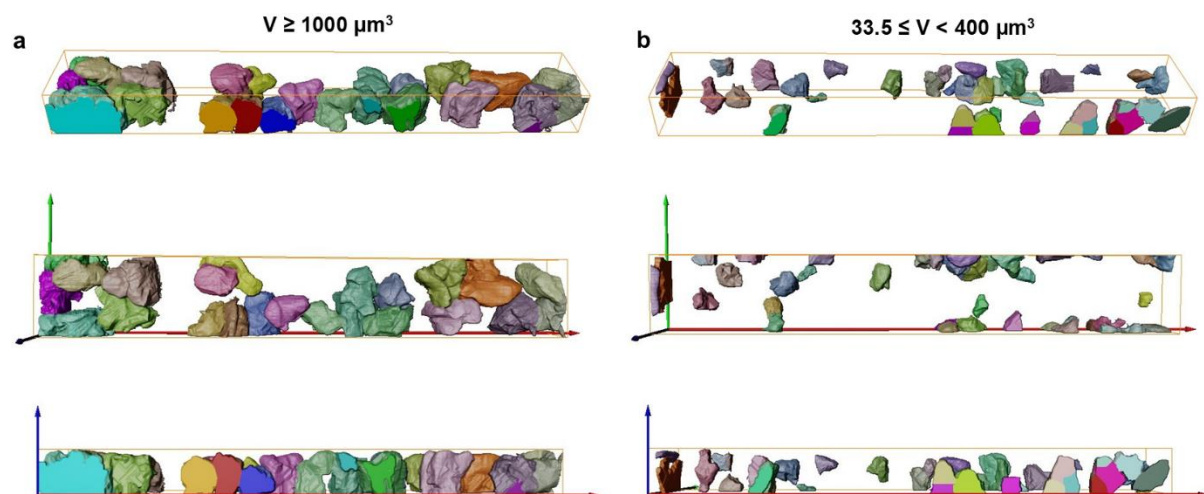


Figure S9. Reconstructed 3D images of separated Li particles at 0.2 mA cm⁻²

(a) Li particle sizes of $V \geq 1000 \mu\text{m}^3$ viewed from different directions.

(b) Li particle sizes of $33.5 \mu\text{m}^3 \leq V < 400 \mu\text{m}^3$ viewed from different directions.

The red, green, and blue arrows indicate the directions of the x-, y-, and z-axes, respectively.

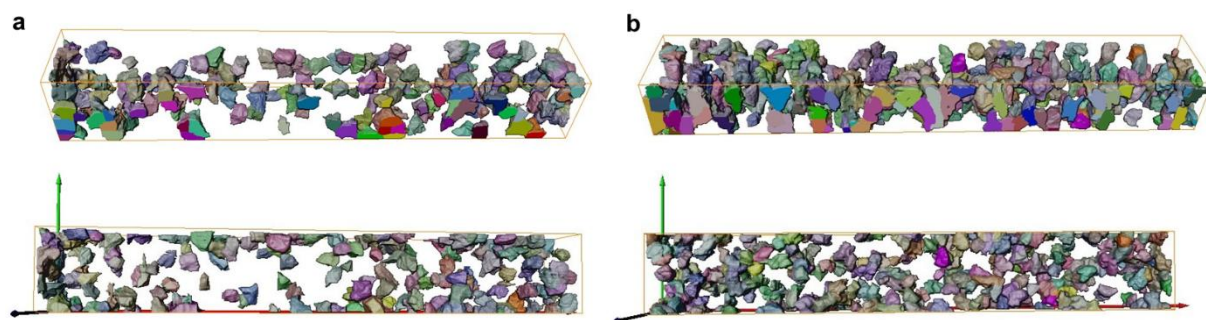


Figure S10. Reconstructed 3D images of Li particles with sizes of $33.5 \mu\text{m}^3 \leq V < 200 \mu\text{m}^3$

(a) The electrodeposited Li obtained at 0.5 mA cm⁻².

(b) The electrodeposited Li obtained at 2 mA cm⁻².

The red, green, and blue arrows indicate the directions of the x-, y-, and z-axes, respectively.

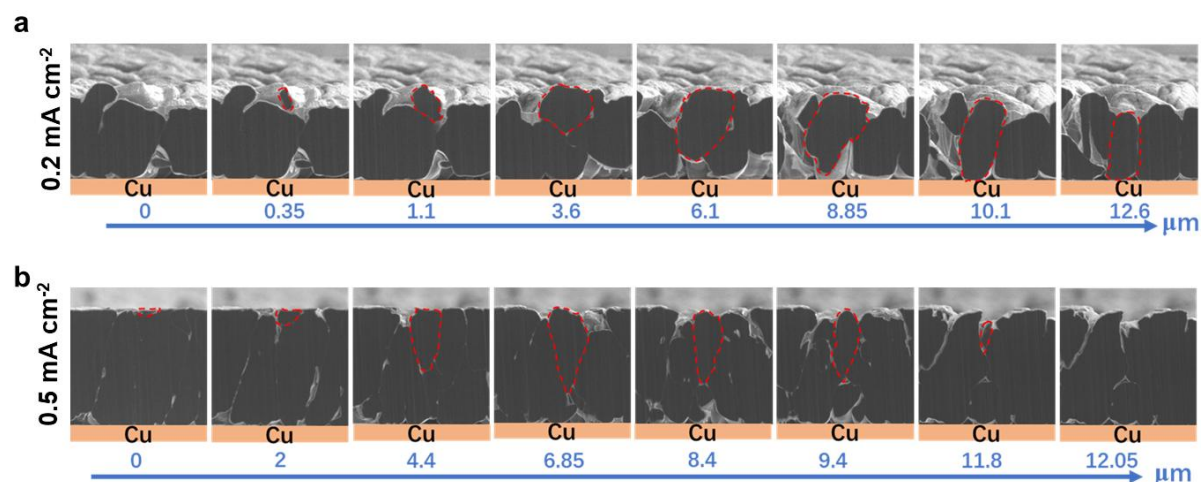


Figure S11. Cross-sectional SEM images of electrodeposited Li metal

(a) The electrodeposited Li obtained at 0.2 mA cm⁻².

(b) The electrodeposited Li obtained at 0.5 mA cm⁻².

The images are acquired by sequentially increasing the distance in the y-axis direction. The red outlines highlight the observed Li particles.

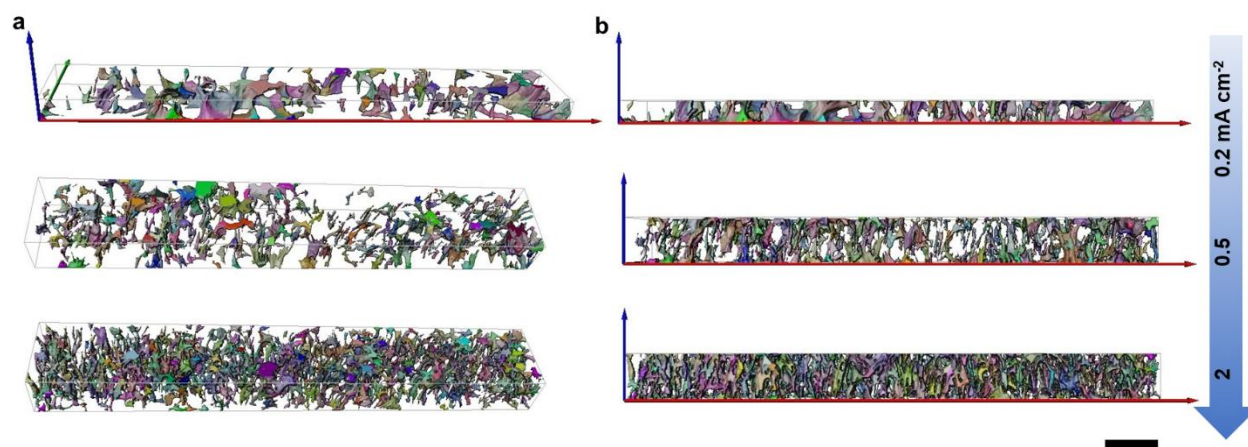


Figure S12. Reconstructed 3D images of separated pores.

(a) Reconstructed volume of the pore structure after cutting the surface with a Li volume fraction of <90%.

(b) Corresponding observation from the front side.

The scale bar represents 20 μm, and the volumes are controlled at the same dimensions of x = 200 μm and y = 30 μm. The red, green, and blue arrows indicate the directions of the x-, y-, and z-axes, respectively.

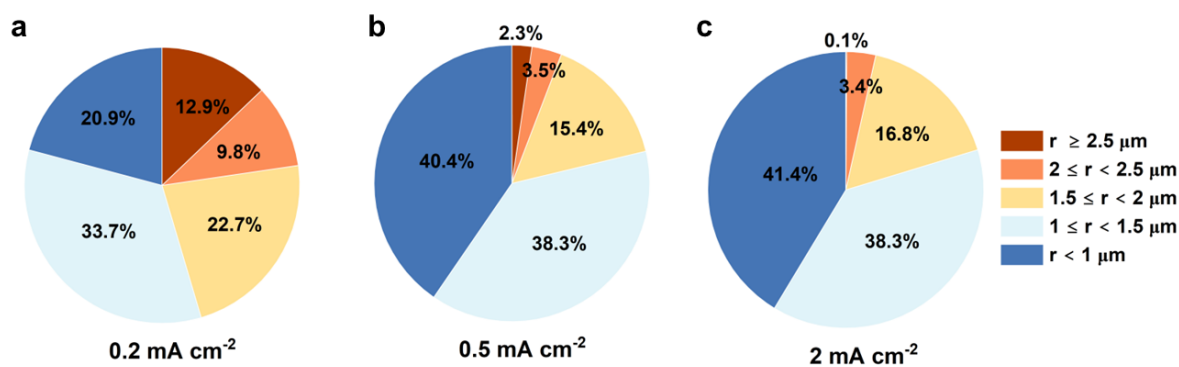


Figure S13. Number percentages of pores in different size ranges

(a) The electrodeposited Li obtained at 0.2 mA cm⁻².

(b) The electrodeposited Li obtained at 0.5 mA cm⁻².

(c) The electrodeposited Li obtained at 2 mA cm⁻².

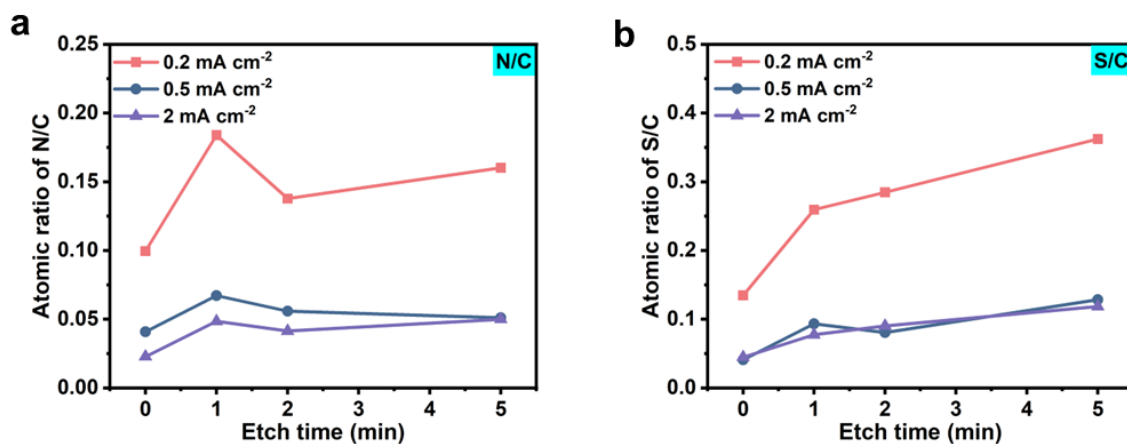


Figure S14. Atomic ratios within the SEIs at different current densities of 0.2, 0.5 and 2 mA cm⁻²

(a) N/C ratios.

(b) S/C ratios.

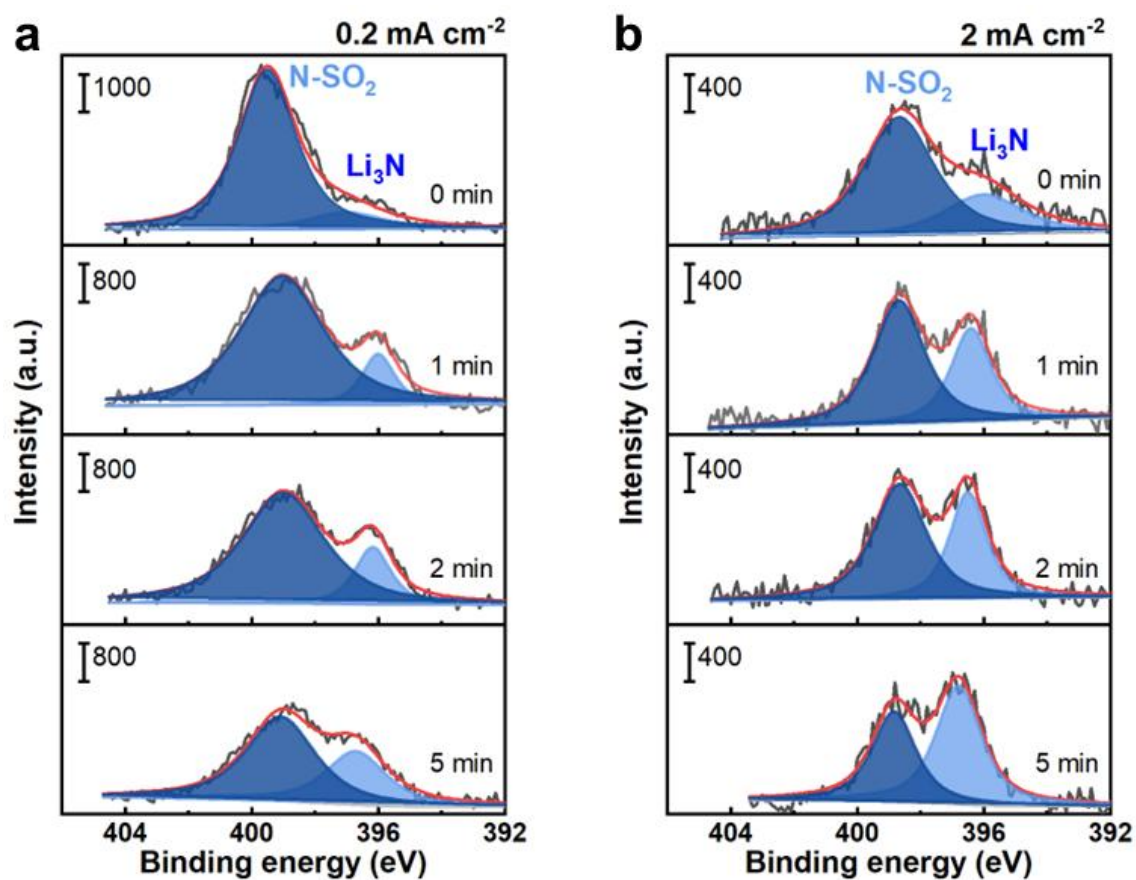


Figure S15. High-resolution N 1s XPS spectra of the SEIs

(a) The electrodeposited Li obtained at 0.2 mA cm⁻².

(b) The electrodeposited Li obtained at 2 mA cm⁻².

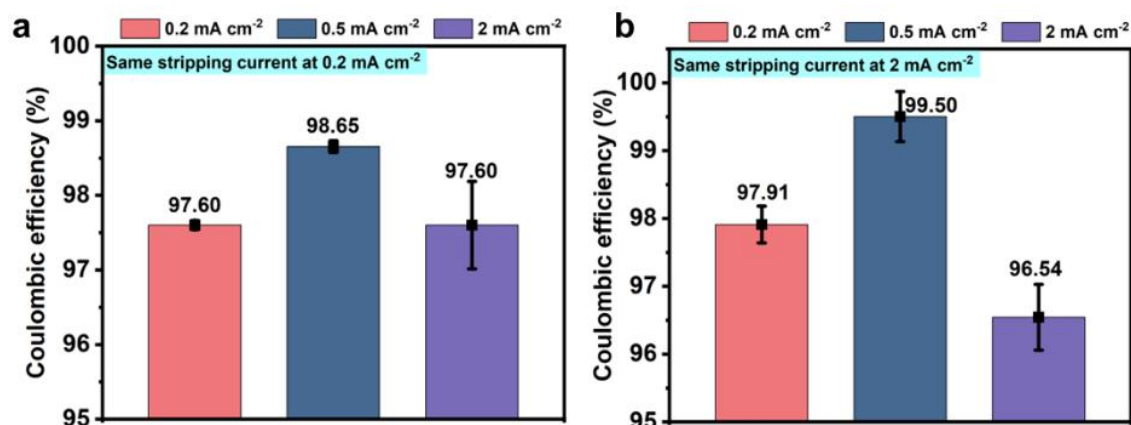


Figure S16. Coulombic efficiencies (CEs) of electrodeposited Li using Li/Cu cells

(a) At the same stripping current density of 0.2 mA cm⁻². The error bars of 0.2, 0.5 and 2 mA cm⁻² are 0.06, 0.08, and 0.59 respectively.

(b) At the same stripping current density of 2 mA cm⁻². The error bars of 0.2, 0.5 and 2 mA cm⁻² are 0.27, 0.37, and 0.48 respectively.

The obtained CEs are averaged over three cells, and each error bar represents one standard deviation.

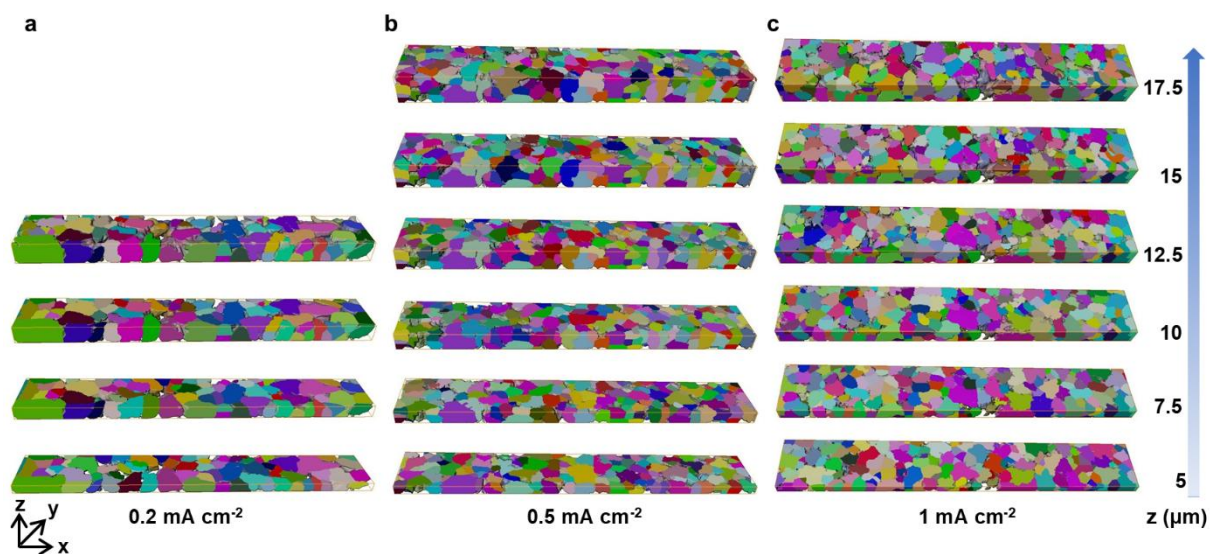


Figure S17. Analyses of the sizes and number of Li particles during Li electrodeposition

(a) Illustration of the analyzed sub-volumes of Li electrodeposited at 0.2 mA cm^{-2} .

(b) Illustration of the analyzed sub-volumes of Li electrodeposited at 0.5 mA cm^{-2} .

(c) Illustration of the analyzed sub-volumes of Li electrodeposited at 1 mA cm^{-2} .

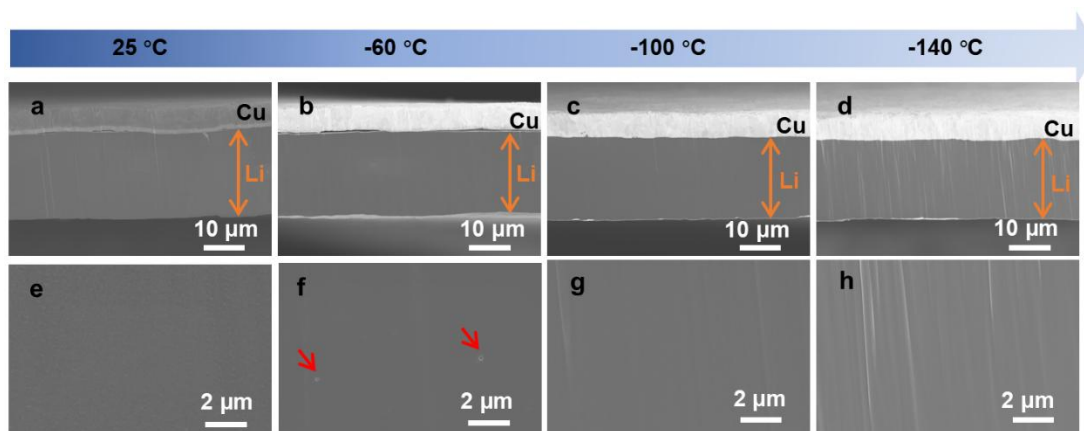


Figure S18. Cross-sectional SEM images of commercial Li metal foil after Xe PFIB cross-sectional milling

(a and e) At temperature of 25 °C.

(b and f) At temperature of -60 °C.

(c and g) At temperature of -100 °C.

(d and h) At temperature of -140 °C.

(e–h) are the magnified images of (a–d), respectively.

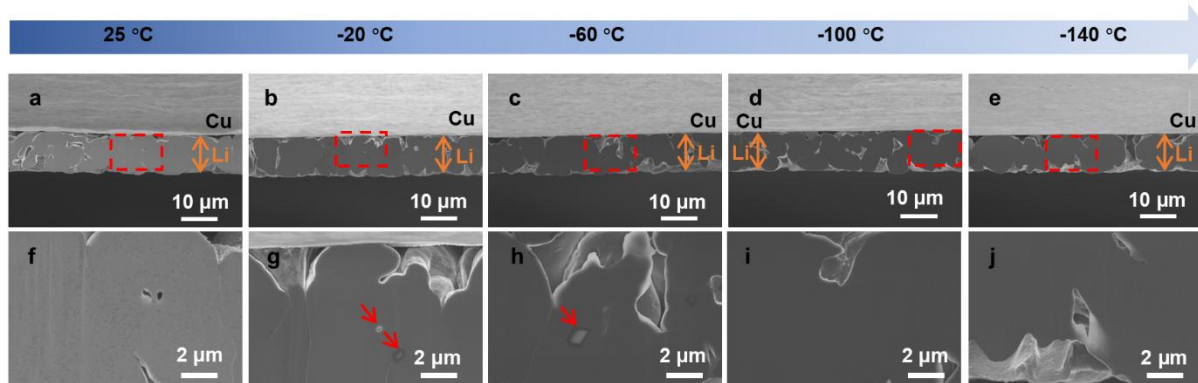


Figure S19. Cross-sectional SEM images of electrodeposited Li after Xe PFIB cross-sectional milling

(a and f) At temperature of 25 °C.

(b and g) At temperature of -20 °C.

(c and h) At temperature of -60 °C.

(d and i) At temperature of -100 °C.

(e and j) At temperature of -140 °C.

(f–j) are the magnified images of (a–e), respectively. The electrodeposited Li was obtained at 0.5 mA cm^{-2} with a capacity of 2 mAh cm^{-2} using 4 M lithium bis(fluorosulfonyl)imide in 1,2-dimethoxyethane as the electrolyte.

Table S1. Descriptions of the quantitative parameters used in this study.

Parameter	Symbol	Description	Formula
Area fraction	-	Fraction of the area over that of the total plane	$\text{area fraction} = \frac{\text{label area}}{gx \times gy}$
Volume fraction	-	Fraction of the volume over the total volume	$\text{volume fraction} = \frac{\text{label volume}}{gx \times gy \times gz}$
Li specific surface area	-	Ratio of the surface area of Li to the volume of Li	
Normalized Li surface area	-	Surface area of Li is normalized over the area of the plane.	$\text{normalize surface area} = \frac{\text{surface area}}{gx \times gy}$
Max. curvature	K _{max}	Maximum value of the curvature	-
Min. curvature	K _{min}	Minimum value of the curvature	-
Mean curvature	H	Integral of the mean curvature, indicating how a surface bends by averaging the curvature in all directions	$H = \frac{\kappa_{max} + \kappa_{min}}{2}$
Volume3d	V _p	Volume of the particle	-
Area3d	A _p	Area of the particle boundary	-
Specific surface	-	Surface:volume ratio of the particle	$\text{specific surface} = \frac{A_p}{V_p}$
Equivalent spherical radius	EqR	Radius of a sphere with the same volume as that of the particle	$\text{EqR} = \sqrt[3]{\frac{3V_p}{4\pi}}$
Sphericity	Ψ	Measure of how close the shape of a particle is to a sphere, where Ψ = 1 is a perfect sphere	$\Psi = \frac{\pi^{1/3} (6V_p)^{2/3}}{A_p}$
Barycenter Z	-	Z coordinate of the center of gravity	-
Tortuosity	T ^a	Measure of how convoluted the paths through the pore space are.	$T = \frac{\sum_{i=0}^n v_i }{\sum_{i=0}^n v_{xi} }$

- a. n represents the number of throats. v_i denotes the fluid velocity through throat i, and v_{xi} is its projection along the flow direction within throat i.

Note S1. The size of Li particles for analysis

Figure S8a displays the histogram of all Li particles. It clearly shows that the number of small Li particles is particularly high. The number and volume percentages of Li particles in the different size ranges are further quantified in **Figure S8b**. The small Li particles ($V < 1 \mu\text{m}^3$) represent a very high number percentage (76%); however, their volume percentage is very low (0.0209%), which indicates that a considerably lower capacity is used to deposit the small Li particles with $V < 1 \mu\text{m}^3$. The corresponding 3D image shown in **Figure S8c** reveals that Li particles with $V < 1 \mu\text{m}^3$ are tiny dots, which can be attributed to image recognition artifacts. The morphologies of Li particles with $V \geq 1 \mu\text{m}^3$ were analyzed based on sphericity in **Figure S8d**. The small Li particles exhibit a wide sphericity distribution. As shown in **Figure S8e**, Li particles with radii of $< 2 \mu\text{m}$ (the corresponding volume is $33.5 \mu\text{m}^3$) clearly display a wide sphericity distribution when using the equivalent spherical radius instead of the volume. The 3D images show that these particles are distributed at the edges of the sampled volume. Therefore, we only counted and analyzed the Li particles with $V \geq 33.5 \mu\text{m}^3$ to reduce the interferences of other factors with the statistical results.

Note S2. The temperature for Xe PFIB cross-sectional milling

As shown in **Figure S18a** and **S18e**, numerous white spots are observed at 25°C , which indicates that the Li metal foil is severely damaged. The damage to the Li metal decreases significantly when the temperature is lowered to -60°C (**Figure S18b** and **S18f**); however, several pores are still detected, as indicated by the red arrows. At -100°C or -140°C (**Figure S18c, S18g** and **S18d, S18h**, respectively), the Li structure remains intact.

Similarly, the electrodeposited Li metal suffers severe damage at 25°C (**Figure S19a** and **S19f**). At -20°C and -60°C (**Figure S19b, S19g** and **S19c, S19h**, respectively), low-level reactions occur in the Li metal, as indicated by the red arrows. When the temperature is lowered to -100°C or -140°C (**Figure S19d, S19i** and **S19e, S19j**, respectively), the Li metal maintains its intact morphological structure. Therefore, the sample stage is cooled to -100°C in this study.